IIT-GAN: IRREGULAR AND INTERMITTENT TIME-SERIES SYNTHESIS WITH GENERATIVE ADVERSARIAL NETWORKS

Anonymous authors
Paper under double-blind review

ABSTRACT

Time-series data is one of the most popular data types in the field of machine learning. For various reasons, there is a strong motivation to synthesize fake time-series data. Several disparate settings for time-series synthesis have been previously solved, ranging from synthesizing time-series without any missing values to time-series of multiple signals with different frequencies. In this paper, we solve the problem of synthesizing irregular and intermittent time-series where values can be missing and may not have specific frequencies, which is far more challenging than existing settings. To this end, we adopt various state-of-the-art deep learning concepts, such as autoencoders (AEs), generative adversarial networks (GANs), neural ordinary differential equations (NODEs), neural controlled differential equations (NCDEs), and so on. Our contribution lies in carefully re-designing those heterogeneous technologies and proposing our unified framework. Our method achieves the state-of-the-art synthesis performance for the irregular and intermittent time-series synthesis task.

1 INTRODUCTION

Time-series data occurs frequently in real-world applications (Reinsel, 2003; Fu, 2011; Li et al., 2018; Yu et al., 2018; Wu et al., 2019; Guo et al., 2019; Bai et al., 2019; Song et al., 2020; Huang et al., 2020; Ren et al., 2021; Tekin et al., 2021). Among many tasks related to time-series, synthesizing time-series data is one of the most important tasks because real-world time-series data is frequently imbalanced and/or insufficient. However, the problem of synthesizing time-series data is still under-explored although the following couple of important problem settings had been studied previously (Yoon et al., 2019; Alaa et al., 2021): i) time-series data does not have any missing values, and ii) time-series data consists of various signals with different frequencies. However, these methods cannot be applied to our case for the reasons which will be described shortly.

In this paper, we solve the problem of synthesizing irregular and intermittent time-series where i) signals at some time-points can be missing and/or ii) signals do not have predetermined frequencies — we focus on this specific problem setting although our method is able to process regular time-series without any model changes. This type of data frequently happens in medical domains for data

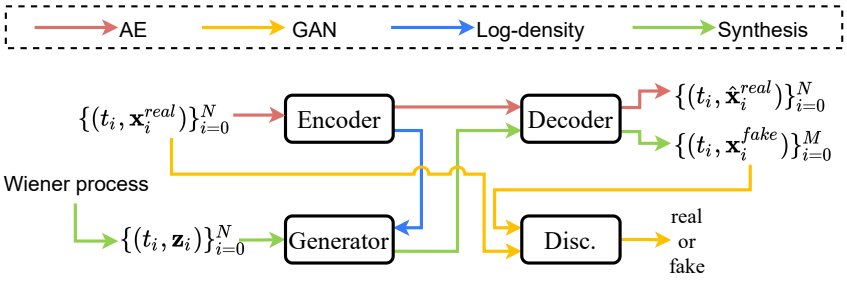

Figure 1: The overall design of the proposed method, IIT-GAN. Each color means each workflow. The autoencoder and the GAN share the workload to synthesize irregular and intermittent time-series.

anonymization (Reyna et al., 2019), battery-powered Internet-of-things applications for elongate the lifetime of battery-powered sensing devices (Ma et al., 2020), and so forth. It is known that neural networks perform better after transforming time-series data into its frequency domain, i.e., the Fourier transform (Alaa et al., 2021). In particular, however, the second characteristic prevents the Fourier transform of time-series from being used as a pre-processing method since it is not easy to observe pre-determined frequencies from highly irregular and intermittent time-series (Kidger et al., 2019).

Our irregular and intermittent time-series setting is different from existing ones. To achieve the goal, therefore, we utilize a diverse set of technology ranging from generative adversarial networks (GANs (Goodfellow et al., 2014)), and autoencoders (AEs) to neural ordinary differential equations (NODEs (Chen et al., 2018)), neural controlled differential equations (NCDEs (Kidger et al., 2020)), and continuous time flow processes (CTFPs (Deng et al., 2020)), which reflects the difficulty of the problem. We show that existing approaches are not as good at synthesizing irregular and intermittent time-series as our proposed method. Since observations are sparse in our setting, we need a sophisticated model to synthesize. In particular our ablation studies in Appendix E justifies our sophisticated design choices.

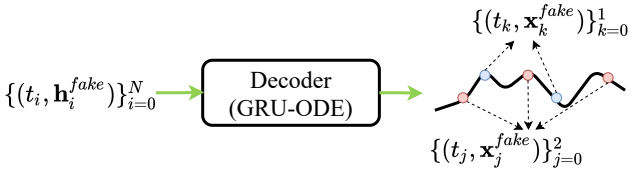

Figure 2: An example of sampling two irregular time-series from a fake continuous path represented by an ordinary differential equation (ODE). In other words, we solve ODE problems to sample irregular time-series.

Fig. 1 shows the overall design of our proposed method. One of the key points in our model design is that we combine the *adversarial* training of GANs and the *exact maximum likelihood* training by the change of variable theorem (Deng et al., 2020) into a single framework. However, the change of variable theorem is applicable only to invertible mapping functions whose input and output sizes are the same. Therefore, we design an *invertible* generator, and adopt an autoencoder, on whose hidden space our GAN performs the adversarial training. In other words, i) the hidden vector size of the encoder is the same as the noisy vector input size of the generator, ii) the generator produces a set of fake hidden vectors, iii) the decoder converts the set into a fake continuous path, and we sample a human-readable (discrete) fake time-series sample (cf. Fig. 2), and iv) the discriminator provides feedback after reading the sampled fake sample. We note that in the third step, a fake continuous path is created by the decoder. Therefore, we can sample any arbitrary irregular/regular time-series sample from the fake path, which shows the flexibility in our method.

We conduct experiments with 4 datasets and 7 baselines. Since our method is able to support both the regular and irregular time-series synthesis, we test for both of them. Our method outperforms them in both environments. Our contributions can be summarized as follows:

1. We design a model based on various state-of-the-art deep learning technologies for time-series. Our method is able to process any types of time-series data, ranging from regular to irregular and intermittent. However, the main novelty lies in processing irregular and intermittent time-series, which has not been solved yet.
2. Our experimental results and visualization prove the efficacy of the proposed model.

2 Related Work and Preliminaries

GANs are one of the most representative generative technology. Ever since the first introduction in its seminal research paper, GANs have been adopted to main different domains. Recently, researchers focused on their synthesis for time-series data. Therefore, there have been proposed several GANs for time-series synthesis.

C-RNN-GAN (Mogren, 2016) has a regular GAN framework that can be applied to sequential data by using LSTM in its generator and discriminator. Recurrent Conditional GAN (RCGAN (Esteban et al., 2017)) took a similar approach except that its generator and discriminator take conditional input for better synthesis. WaveNet (van den Oord et al., 2016) also generates time-series data from the conditional probability of previous data by using the dilated casual convolution. WaveGAN (Donahue

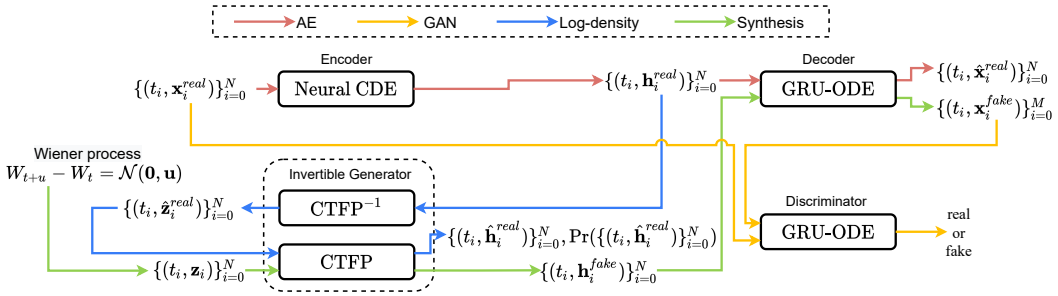

Figure 3: The detailed architecture of our proposed method. Neural CDEs (or NCDEs) are a recent breakthrough for processing time-series. GRU-ODEs are a continuous interpretation of gated recurrent units (GRUs) based on NODEs. CTFPs are a flow-based concept to convert an input time-series process into a target process. CTFPs are not a GAN-based concept but we integrate them into our framework, considering the challenging nature of the irregular and intermittent time-series synthesis.

et al., 2019) has a similar approach with DCGAN (Radford et al., 2016), where its generator is based on WaveNet. We can modify the teacher-forcing (T-Forcing (Graves, 2014)) and professor-forcing (P-Forcing (Lamb et al., 2016)) models to generate time-series data from noise vectors, although they are not GAN models, by using the forecasting characteristic of those models.

TimeGAN (Yoon et al., 2019) is yet another model for time-series synthesis. This model aims mainly at synthesizing fake *regular* time-series samples. They proposed a framework where the adversarial training of GANs and the supervised training of predicting $\mathbf{x}_{i+1}$ from $\mathbf{x}_i$, where $\mathbf{x}_i$ and $\mathbf{x}_{i+1}$ mean two multivariate time-series values at time t_i and t_{i+1}, respectively.

FourierFlow (FF (Alaa et al., 2021)) significantly enhances the applicability of the time-series synthesis technology toward the complicated case where multiple signals with different frequencies are mixed into time-series samples. Some other models assume that all signals have the same frequency whereas FF does not. With conventional deep learning models, it is not straightforward to process signals with different frequencies and therefore, they propose to transform time-series samples into their frequency domain and synthesize. This approach shows high synthesis performance for their purposes.

Stochastic differential equations (SDEs) are preferred to mathematically model temporal dynamics in some special cases. Neural SDEs were proposed to learn SDEs with *continuous* time from data (Kidger et al., 2021) and after that, the fitted SDEs can be used to synthesize temporal dynamics. Although some methods tried to overcome the limitation, it is still unknown that it can be used for a wide variety of time-series data (Kidger et al., 2021).

3 Proposed Method

We describe our detailed design. Since our irregular and intermittent time-series synthesis is a challenging task, the proposed design is much more complicated than other baselines.

3.1 Overall Workflow

We first describe the overall workflow in our model design, which consists of several different data paths (and several different training methods based on the data paths) as follows:

1. **Autoencoder Path:** Given an irregular time-series sample $\{(t_i, \mathbf{x}_i^{real})\}_{i=0}^N$, where $\mathbf{x}_i^{real}$ is a vector denoting values at time t_i, the encoder produces a set of hidden vectors $\{\mathbf{h}_i^{real}\}_{i=0}^N$. The decoder recovers a continuous path $\hat{X}^{real}$, which enhances the flexibility of our proposed method. From the path $\hat{X}^{real}$, we sample $\{(t_i, \hat{\mathbf{x}}_i^{real})\}_{i=0}^N$. We train the encoder and the decoder using the standard autoencoder (AE) loss to match $\mathbf{x}_i^{real}$ and $\hat{\mathbf{x}}_i^{real}$ for all i.
2. **Adversarial Path:** Given a set of noisy vectors $\{\mathbf{z}_i\}_{i=0}^N$, our generator produces a set of fake hidden vectors $\{\mathbf{h}_i^{fake}\}_{i=0}^N$. The decoder recovers a fake continuous path $\hat{X}^{fake}$ from

$\{\mathbf{h}_i^{fake}\}_{i=0}^N$. We sample $\{(t_j, \mathbf{x}_j^{fake})\}_{j=0}^M$ from $\hat{X}^{fake}$ and feed it into the discriminator. Given a time domain $[0, T]$, we randomly sample t_j to construct the irregular time-series sample. We train the generator, the decoder, and the discriminator using the standard adversarial loss.

3. **Log-density Path:** Given a set of hidden vectors $\{\mathbf{h}_i^{real}\}_{i=0}^N$ for an irregular time-series sample $\{(t_i, \mathbf{x}_i^{real})\}_{i=0}^N$, the inverse path of the generator reproduces a set of noisy vectors $\{\hat{\mathbf{z}}_i\}_{i=0}^N$. We feed $\{\hat{\mathbf{z}}_i\}_{i=0}^N$ into its forward path again to reproduce $\{\hat{\mathbf{h}}_i^{real}\}_{i=0}^N$, where $\hat{\mathbf{h}}_i^{real} = \mathbf{h}_i^{real}$ for all i. During the forward pass, we calculate the negative log probability of $-\log p(\hat{\mathbf{h}}_i^{real})$ for all i with the change of variable theorem and minimize it for training.

Being inspired by Flow-Gan (Grover et al., 2018), we also combine the adversarial training and the exact likelihood training. In particular, we note that the dimensionality of the hidden space of the autoencoder is the same as that of the latent input space of the generator, i.e., $\dim(\mathbf{h}) = \dim(\mathbf{z})$. This is needed for the exact likelihood training in the generator — the change of variable theorem requires that the input and output sizes are the same to estimate the exact likelihood. In addition to it, we let the autoencoder and the generator share the workload to synthesize fake time-series by combining them into a single framework, i.e., the generator synthesizes fake hidden vectors and the decoder reproduces human-readable fake time-series from them.

3.2 AUTOENCODER

Encoder General NCDEs, which are considered as a continuous analogue to recurrent neural networks (RNNs), are defined as follows:

$$\mathbf{h}(t_{i+1}) = \mathbf{h}(t_i) + \int_{t_i}^{t_{i+1}} f(\mathbf{h}(t); \theta_f) dX(t) = \mathbf{h}(t_i) + \int_{t_i}^{t_{i+1}} f(\mathbf{h}(t); \theta_f) \frac{dX(t)}{dt} dt, \tag{1}$$

where $X(t)$ is a continuous path created from a raw discrete time-series sample $\{(t_i, \mathbf{x}_i^{real})\}_{i=0}^N$ by an interpolation algorithm — we note that $X(t_i) = (t_i, \mathbf{x}_i^{real})$ for all i, and for other non-observed time-points the interpolation algorithm fills out values. Note that NCDEs keep reading the time-derivative of $X(t)$, denoted $\dot{X}(t) \overset{\text{def}}{=} \frac{dX(t)}{dt}$. In our case, we collect $\mathbf{h}_i^{real}$ for all i, denoted $\{\mathbf{h}_i^{real}\}_{i=0}^N$, as follows:

$$\mathbf{h}_{i+1}^{real} = \mathbf{h}_i^{real} + \int_{t_i}^{t_{i+1}} f(\mathbf{h}(t); \theta_f) \frac{dX(t)}{dt} dt, \tag{2}$$

where $\mathbf{h}_0^{real} = \texttt{FC}_{\dim(\mathbf{x}) \to \dim(\mathbf{h})}(\mathbf{x}_0^{real})$ and $\texttt{FC}_{input\_size \to output\_size}$ is a fully-connected layer with specific input and output sizes. We refer to Appendix for the ODE function f definition.

Therefore, the input time-series $\{(t_i, \mathbf{x}_i^{real})\}_{i=0}^N$ is represented by a set of hidden vectors $\{(t_i, \mathbf{h}_i^{real})\}_{i=0}^N$. Because NCDEs are a continuous analogue to RNNs, it shows the best fit to processing irregular time-series (Kidger et al., 2020).

Decoder Our decoder, which reproduces a time-series from its hidden representations, is based on GRU-ODEs (Brouwer et al., 2019) and is defined as follows:

$$\bar{\mathbf{d}}(t_{i+1}) = \mathbf{d}(t_i) + \int_{t_i}^{t_{i+1}} g(\mathbf{d}(t), t; \theta_g) dt, \tag{3}$$

$$\mathbf{d}(t_{i+1}) = \texttt{GRU}(\mathbf{h}_{i+1}, \bar{\mathbf{d}}(t_{i+1})), \tag{4}$$

$$(t_{i+1}, \hat{\mathbf{x}}_{i+1}) = (t_{i+1}, \texttt{FC}_{\dim(\mathbf{d}) \to \dim(\mathbf{x})}(\mathbf{d}(t_{i+1}))), \tag{5}$$

where $\mathbf{d}(t_0) = \texttt{FC}_{\dim(\mathbf{h}) \to \dim(\mathbf{d})}(\mathbf{h}_0)$ and $\mathbf{h}_i$ means either the i-th real or fake hidden vector, i.e., $\mathbf{h}_i^{real}$ or $\mathbf{h}_i^{fake}$ — recall that in Fig. 3, the decoder is involved in both the autoencoder and the synthesis processes. $\hat{\mathbf{x}}$ means a reproduced copy of $\mathbf{x}$. GRU-ODEs uses the technology called neural ordinary differential equations (NODEs) to *continuously* interpret GRUs and we refer to Appendix for the ODE function g definition.

In particular, the gated recurrent unit (GRU) at Eq. 4 is called as *jump* which is known to be effective in processing time-series with NODEs (Brouwer et al., 2019; Jia & Benson, 2019). We train the encoder-decoder using the standard reconstruction loss between $\mathbf{x}_i^{real}$ and $\hat{\mathbf{x}}_i^{real}$ for all t_i in all training time-series samples.

3.3 GENERATIVE ADVERSARIAL NETWORK

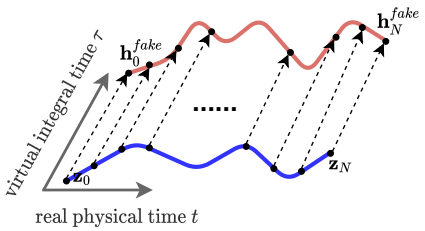

Figure 4: An example of our generation

Generator Whereas generators typically read a noisy vector to generate a fake sample in standard GANs, our generator reads a continuous path (or time-series) sampled from a Wiener process to generate a fake time-series sample — this generation concept is known as continuous time flow processes (CTFPs (Deng et al., 2020)). Fig. 4 shows an example of our generation process. The input to our generation process is a random path sampled from a Wiener process, which is represented by a time-series of latent vectors $\{(t_i, \mathbf{z}_i)\}_{i=0}^N$ in the path, and the output is a path of hidden vectors which is also represented by a time-series of hidden vectors $\{(t_i, \mathbf{h}_i^{fake})\}_{i=0}^N$. Therefore, our generator can be written as follows:

$$\mathbf{h}_i^{fake} = \mathbf{w}_i(1) = \mathbf{w}_i(0) + \int_0^1 r(\mathbf{w}_i(\tau), a_i(t), t; \theta_r) d\tau, \tag{6}$$

where $\mathbf{w}_i(0) = \mathbf{z}_i$, $a_i(0) = t_i$. Here, τ means a virtual time variable of the integral problem, and t_i is a real physical time contained in a time-series sample $\{(t_i, \mathbf{x}_i^{real})\}_{i=0}^M$. We note that this design corresponds to a NODE model augmented with $a_i(t)$. We refer to Appendix for the ODE function r definition.

Owing to the invertible nature of NODEs, we can calculate the exact log-density of $\mathbf{h}_i^{real}$, i.e., the probability that $\mathbf{h}_i^{real}$ is generated by the generator, using the change of variable theorem and the Hutchinson's stochastic trace estimator as follows (Grathwohl et al., 2019; Deng et al., 2020):

$$\hat{\mathbf{w}}(0) = \mathbf{h}_i^{real} + \int_1^0 r(\mathbf{w}(\tau), a_i(\tau), t; \theta_r) d\tau, \tag{7}$$

$$\log \Pr(\hat{\mathbf{h}}_i^{real}) = \log \Pr(\hat{\mathbf{w}}(0)) + \int_0^1 tr\Big(\frac{\partial r(\mathbf{w}(\tau), a_i(\tau), t; \theta_r)}{\partial \mathbf{w}(\tau)}\Big) d\tau, \tag{8}$$

where $\hat{\mathbf{w}}(0)$ means $\hat{\mathbf{z}}_i^{real}$ in Fig. 3. $\hat{\mathbf{h}}_i^{real}$ means a reproduced copy of $\mathbf{h}_i^{real}$ by our generator. Eq. 7 corresponds to "CTFP^{-1}", and Eqs. 6 and 8 to "CTFP" in Fig. 3. We note that in Eq. 7, the integral time is reversed to solve the reverse-mode integral problem.

Therefore, we minimize the negative log-density, denoted $-\log \Pr(\hat{\mathbf{h}}_i^{real})$, for each t_i, and our generator is trained by the two different training paradigms: i) the adversarial training against the discriminator, and ii) the maximum likelihood estimator (MLE) training with the log-density.

Discriminator We design our discriminator based on the GRU-ODE technology as follows:

$$\bar{\mathbf{c}}(t_{i+1}) = \mathbf{c}(t_i) + \int_{t_i}^{t_{i+1}} q(\mathbf{c}(t), t; \theta_q) dt, \tag{9}$$

$$\mathbf{c}(t_{i+1}) = \texttt{GRU}(\mathbf{x}_{i+1}, \bar{\mathbf{c}}(t_{i+1})), \tag{10}$$

where $\mathbf{c}(t_0) = \texttt{FC}_{\dim(\mathbf{x})\to\dim(\mathbf{c})}(\mathbf{x}_0)$, and $\mathbf{x}_i$ means the i-th time-series value, i.e., $\mathbf{x}_i^{real}$ or $\mathbf{x}_i^{fake}$. The ODE function q has the same architecture as g but with its own parameters θ_q. After that, we calculate the real or fake classification $\mathbf{y} = \sigma(\texttt{FC}_{\dim(\mathbf{c})\to 2}(\mathbf{c}(t_N)))$, where σ is a softmax activation.

3.4 TRAINING METHOD

We use the mean squared reconstruction loss, i.e., the mean of $\|\mathbf{x}_i^{real} - \hat{\mathbf{x}}_i^{real}\|_2^2$ for all t_i of all training samples, to train the encoder-decoder architecture. Then, we use the standard GAN loss to train the generator and the discriminator. In our preliminary experiments, we found that the original GAN loss is suitable for our task. Instead of other variations, such as WGAN-GP (Gulrajani et al., 2017), therefore, we use the standard GAN loss. We train our model in the following sequence:

1. We pre-train the encoder-decoder networks the reconstruction loss for K_{AE} iterations.

2. After the above pre-training step, we start to jointly train all networks in the following sequence for K_{JOINT} iterations: i) training the encoder-decoder networks with the reconstruction loss, ii) training the discriminator-generator networks with the GAN loss, iii) training the decoder to improve the discriminator's classification output with the discriminator loss and iv) the generator with the MLE loss every P_{MLE} iteration. We found that too frequent MLE training incurs mode-collapse so we use it every P_{MLE} iteration.

In particular, the 2-ii step to train the decoder to help the discriminator out is one additional point where the autoencoder and the GAN are integrated into a single framework. In other words, the generator should deceive both the decoder and the discriminator.

The well-posedness[1] of NCDEs and GRU-ODEs was already proved in (Lyons et al., 2007, Theorem 1.3) and (Brouwer et al., 2019) under the mild condition of the Lipschitz continuity. We show that our NCDE layers are also well-posed problems. Almost all activations, such as ReLU, Leaky ReLU, SoftPlus, Tanh, Sigmoid, ArcTan, and Softsign, have a Lipschitz constant of 1. Other common neural network layers, such as dropout, batch normalization and other pooling methods, have explicit Lipschitz constant values. Therefore, the Lipschitz continuity of ODE/CDE functions can be fulfilled in our case. Therefore, it is a well-posed training problem. Therefore, our training algorithm solves a well-posed problem so its training process is stable in practice.

4 Experimental Evaluations

Our software and hardware environments are as follows: Ubuntu 18.04 LTS, Python 3.8.10, Pytorch 1.8.1, Tensorflow 2.5.0, CUDA 11.2, and NVIDIA Driver 417.22, i9 CPU, and NVIDIA RTX 3090. The mean and variance of 10 different seeds are reported for model evaluation.

4.1 Experimental Environments

Datasets We conduct experiments with 2 simulated and 2 real-world datasets. Sines has 5 features where each feature is created with different frequencies and phases independently. For each feature, $i \in \{1, ..., 5\}$, $x_i(t) = sin(2\pi f_i t + \theta_i)$, where $f_i \sim \mathcal{U}[0, 1]$ and $\theta_i \sim \mathcal{U}[-\pi, \pi]$. MuJoCo is multivariate physics simulation time-series data with 14 features. Stocks is the Google stock price data from 2004 to 2019. Each observation represents one day and has 6 features. Energy is a UCI appliance energy prediction dataset with 28 values. To create the challenging irregular and intermittent environments, 30, 50, 70% of observations from each time-series sample $\{(t_i, \mathbf{x}_i^{real})\}_{i=0}^{N}$ is randomly dropped — in other words, N decreases to $0.7N, 0.5N, 0.3N$, respectively. Therefore, we conduct experiments with both the regular and the irregular environments.

Baselines We consider the following baselines for the regular time-series experiments: TimeGAN, RCGAN, C-RNN-GAN, WaveGAN, WaveNet, T-Forcing, and P-Forcing. For the irregular experiments, we exclude WaveGAN and WaveNet, which cannot handle irregular time-series, and redesign other baselines by replacing their GRU with GRU-Decay (GRU-D). TimeGAN-D, RCGAN-D, C-RNN-GAN-D, T-Forcing-D, and P-Forcing-D are those modified with GRU-D and can handle irregular time-series.

Evaluation Metrics For quantitative evaluation of synthesized data, it is evaluated with the discriminative score and the predictive score used in TimeGAN (Yoon et al., 2019). The discriminative score measures the similarity between the original data and the synthesized data. After learning a model that classifies the original data and the synthesized data using a neural network, it is tested whether the original data and the synthesized data are classified well. The discriminative score is |Accuracy-0.5|, and if the score is low, classification is difficult, so the original data and the synthesized data are decided to be similar. The predictive score measures the effectiveness of the synthesized data using the train-synthesis-and-test-real (TSTR) method. After training a model that predicts the next step using the synthesized data, the mean absolute error (MAE) is calculated between the predicted values and the ground-truth values in test data. If the MAE is small, the model trained using the synthesized data is decoded to be similar to the original data. For qualitative evaluation, the synthetic data is

[1] A well-posed problem means i) its solution uniquely exists, and ii) its solution continuously changes as input data changes.

Table 1: Regular time-series

	Method	Sines	Stocks	Energy	MuJoCo
Discriminative Score	IIT-GAN	.012±.014	**.077±.031**	**.221±.068**	**.245±.029**
	TimeGAN	**.011±.008**	.102±.021	.236±.012	.409±.028
	RCGAN	.022±.008	.196±.027	.336±.017	.436±.012
	C-RNN-GAN	.229±.040	.399±.028	.499±.001	.412±.095
	T-Forcing	.495±.001	.226±.035	.483±.004	.499±.000
	P-Forcing	.430±.227	.257±.026	.412±.006	.500±.000
	WaveNet	.158±.011	.232±.028	.397±.010	.385±.025
	WaveGAN	.277±.013	.217±.022	.363±.012	.357±.017
Predictive Score	IIT-GAN	.097±.000	.040±.000	.312±.002	**.055±.000**
	TimeGAN	**.093±.019**	.038±.001	**.273±.004**	.082±.006
	RCGAN	.097±.001	.040±.001	.292±.005	.081±.003
	C-RNN-GAN	.127±.004	**.038±.000**	.483±.005	.055±.004
	T-Forcing	.150±.022	.038±.001	.315±.005	.142±.014
	P-Forcing	.116±.004	.043±.001	.303±.006	.102±.013
	WaveNet	.117±.008	.042±.001	.311±.005	.333±.004
	WaveGAN	.134±.013	.041±.001	.307±.007	.324±.006
	Original	.094±.001	.036±.001	.250±.003	.031±.003

Table 2: Irregular time-series (30% dropped)

	Method	Sines	Stocks	Energy	MuJoCo
Disc. Score	IIT-GAN	**.363±.063**	**.251±.097**	**.333±.063**	**.249±.035**
	TimeGAN-D	.496±.008	.411±.040	.479±.010	.463±.025
	RCGAN-D	.500±.000	.500±.000	.500±.000	.500±.000
	C-RNN-GAN-D	.500±.000	.500±.000	.500±.000	.500±.000
	T-Forcing-D	.408±.087	.409±.051	.347±.046	.494±.004
	P-Forcing-D	.500±.000	.480±.060	.491±.020	.500±.000
Predictive Score	IIT-GAN	**.099±.004**	**.021±.003**	**.066±.001**	**.048±.001**
	TimeGAN-D	.192±.082	.105±.053	.248±.024	.098±.006
	RCGAN-D	.388±.113	.523±.020	.409±.020	.361±.073
	C-RNN-GAN-D	.664±.001	.345±.002	.440±.000	.457±.001
	T-Forcing-D	.100±.002	.027±.002	.090±.001	.100±.001
	P-Forcing-D	.154±.004	.079±.008	.147±.001	.173±.002
	Original	.071±..004	.011±.002	.045±.001	.041±.002

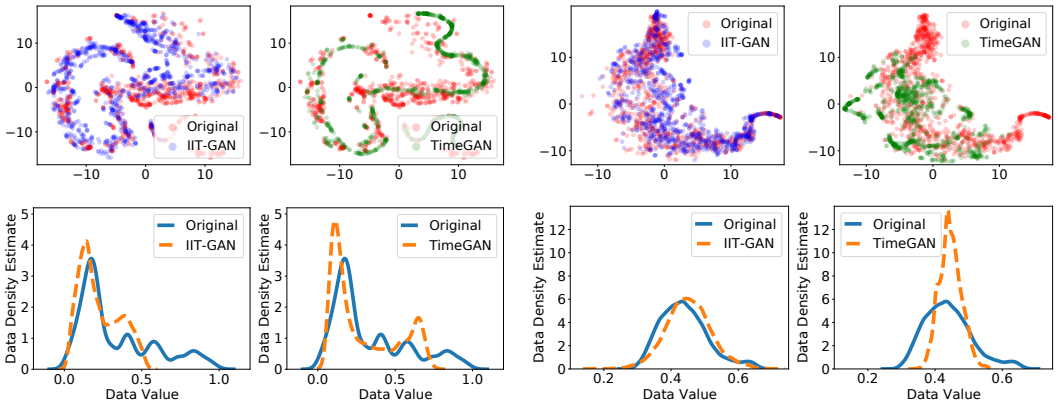

(a) Stocks (b) Energy

Figure 5: Visualizations and distributions of the regular time-series synthesized by IIT-GAN and TimeGAN. Other visualizations are in Appendix.

visualized with the original data. There are two methods for visualization. One is to project original and synthetic data in a two dimensional space using t-SNE (Van der Maaten & Hinton, 2008). The other one is the kernel density estimation to draw data distributions.

4.2 Experimental Results

Regular Time-series Synthesis In Table 1, we list the results of the regular time-series synthesis. IIT-GAN shows better performance on most cases than TimeGAN, the previous state-of-the-art model. As shown in the 1st row in Fig. 5, IIT-GAN covers original data areas better than TimeGAN. In addition, the 2nd row in Fig. 5 is the distributions of the fake data generated by IIT-GAN and TimeGAN. The synthesized data's distributions from IIT-GAN are more similar to those of the original data than TimeGAN, which shows the efficacy of the *explicit* likelihood training of IIT-GAN against the *implicit* likelihood training of TimeGAN.

Irregular and Intermittent Time-series Synthesis In Tables 2, 3, and 4, we list the results of the irregular and intermittent time-series synthesis. IIT-GAN shows better discriminative and predictive scores than other baselines in all cases. In Table 2, where we drop random 30% of observations from each time-series sample, IIT-GAN shows the best outcomes, outperforming TimeGAN by large margins. In Table 3 (50% dropped), many baselines do not show reasonable synthesis quality, e.g., TimeGAN-D, RCGAN-D, and C-RNN-GAN-D have a discriminative score of 0.5. Surprisingly, T-Forcing-D and P-Forcing-D work well in this case. However, our model clearly shows the best performance in all datasets. Finally, Table 4 (70% dropped) shows the results of the most challenging

Table 3: Irregular time-series (50% dropped)

	Method	Sines	Stocks	Energy	MuJoCo
Disc. Score	IIT-GAN	**.372±.128**	**.265±.073**	**.317±.010**	**.270±.016**
	TimeGAN-D	.500±.000	.477±.021	.473±.015	.500±.000
	RCGAN-D	.500±.000	.500±.000	.500±.000	.500±.000
	C-RNN-GAN-D	.500±.000	.500±.000	.500±.000	.500±.000
	T-Forcing-D	.430±.101	.407±.034	.376±.046	.498±.001
	P-Forcing-D	.499±.000	.500±.000	.500±.000	.500±.000
Predictive Score	IIT-GAN	**.101±.010**	**.018±.002**	**.064±.001**	**.056±.003**
	TimeGAN-D	.169±.074	.254± .047	.339±.029	.375±.011
	RCGAN-D	.519±.046	.333±.044	.250±.010	.314±.023
	C-RNN-GAN-D	.754±.000	.273±.000	.438±.000	.479±.000
	T-Forcing-D	.104±.001	.038±.003	.090±.000	.113±.001
	P-Forcing-D	.190±.002	.089±.010	.198±.005	.207±.008
	Original	.071±.004	.011±.002	.045±.001	.041±.002

Table 4: Irregular time-series (70% dropped)

	Method	Sines	Stocks	Energy	MuJoCo
Disc. Score	IIT-GAN	**.278±.022**	**.230±.053**	**.325±.047**	**.275±.023**
	TimeGAN-D	.498±.006	.485±.022	.500±.000	.492±.009
	RCGAN-D	.500±.000	.500±.000	.500±.000	.500±.000
	C-RNN-GAN-D	.500±.000	.500±.000	.500±.000	.500±.000
	T-Forcing-D	.436±.067	.404±.068	.336±.032	.493±.005
	P-Forcing-D	.500±.000	.449±.150	.494±.011	.499±.000
Predictive Score	IIT-GAN	**.088±.005**	**.020±.005**	**.076±.001**	**.051±.001**
	TimeGAN-D	.752±.001	.228±.000	.443±.000	.372±.089
	RCGAN-D	.404±.034	.441±.045	.349±.027	.420±.056
	C-RNN-GAN-D	.632±.001	.281±.019	.436±.000	.479±.001
	T-Forcing-D	.102±.001	.031±.002	.091±.000	.114±.003
	P-Forcing-D	.278±.045	.107±.009	.193±.006	.191±.005
	Original	.071±..004	.011±.002	.045±.001	.041±.002

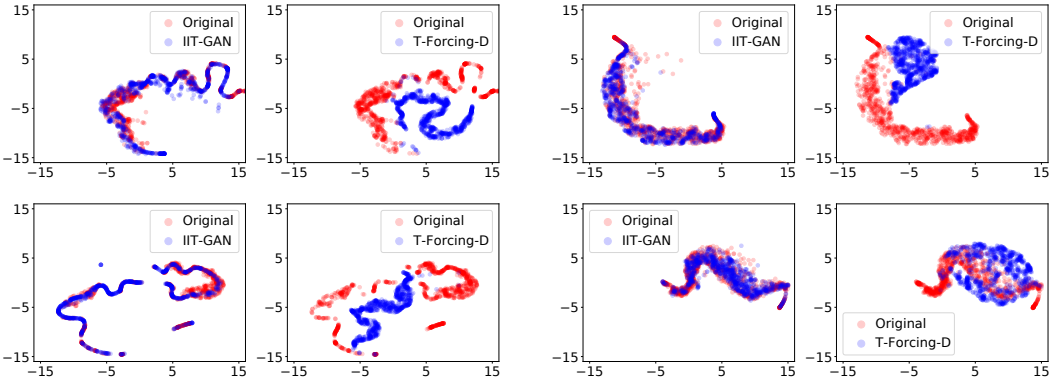

(a) Stocks (b) Energy

Figure 6: Visualizations of the irregular time-series synthesized by IIT-GAN and T-Forcing-D (the 1st row is for a dropping rate of 30%, and the 2nd row for a rate of 50%)

experiments in our paper. All baselines do not work well because of the high dropping rate. T-Forcing-D and P-Forcing-D, which showed reasonable performance with a dropping rate no larger than 50%, do not work well in this case. This shows that they are vulnerable to highly irregular and intermittent time-series data. Other GAN-based baselines are vulnerable as well. Our method greatly outperforms all existing methods, e.g., a predictive score of 0.051 by IIT-GAN vs. 0.114 by T-Forcing-D, the best performing baseline, for MuJoCo. Figs. 6 and 7 visually compare our method and the best performing baseline in each experiment.

Ablation & Sensitivity Analyses IIT-GAN is characterized by the MLE training with the negative log-density in Eq. 8, and the pre-training step of the encoder and decoder. Table 5 shows the results of the modified IIT-GANs with each training mechanism removed, respectively. The model using the negative log-density training shows better performance than the model not using it. That is, the MLE training makes the synthetic data more like the real data. When the pre-trained autoencoder model is not used, the predictive score is better than the existing IIT-GAN. However, the discriminative score is the worst. The hyperparameters that significantly affect model performance are the absolute tolerance (atol), the relative tolerance (rtol), and the period of the MLE training (P_{MLE}) for the generator. The atol and rtol determine the error control performed by the ODE solvers in CTFPs. We test with various options of the hyperparameters in Fig 8. We found that there is an appropriate error tolerance (atol, rtol) depending on the data input size. For example, datasets with small input sizes (Sines, Stocks) have good discriminator scores with (1e-2, 1e-3), and datasets with large input sizes (Energy, MuJoCo) show good results with (1e-3, 1e-2).

Table 5: Ablation study. See Appendix E for other ablation studies.

	Method (Regular)	Sines	Stocks	Energy	MuJoCo
Disc.	IIT-GAN	**.012**	**.077**	**.221**	**.245**
	w/o Eq. 8	.023	.159	.356	.278
	w/o pre-training	.046	.175	.312	.290
Pred.	IIT-GAN	.097	.040	.312	.055
	w/o Eq. 8	.097	.043	.315	.057
	w/o pre-training	**.096**	**.038**	**.299**	**.052**

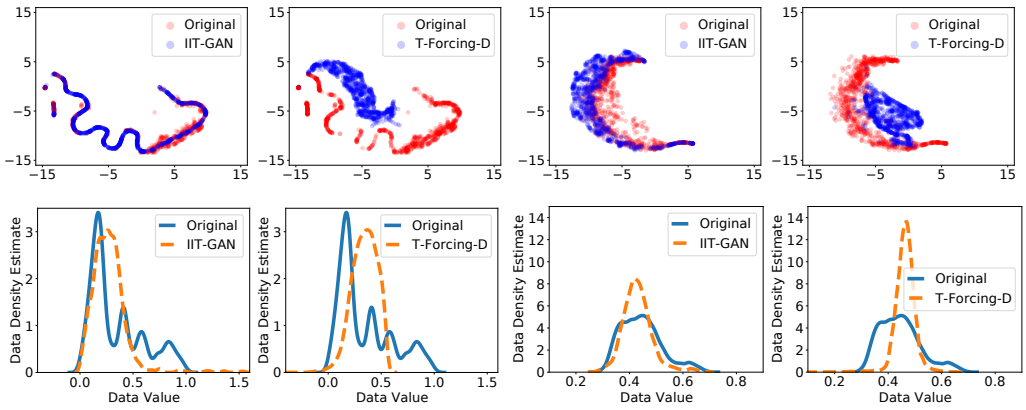

(a) Stocks (b) Energy

Figure 7: Visualizations of the irregular time-series (70% dropped) synthesized by IIT-GAN (the 1st row) and T-Forcing-D (the 2nd row)

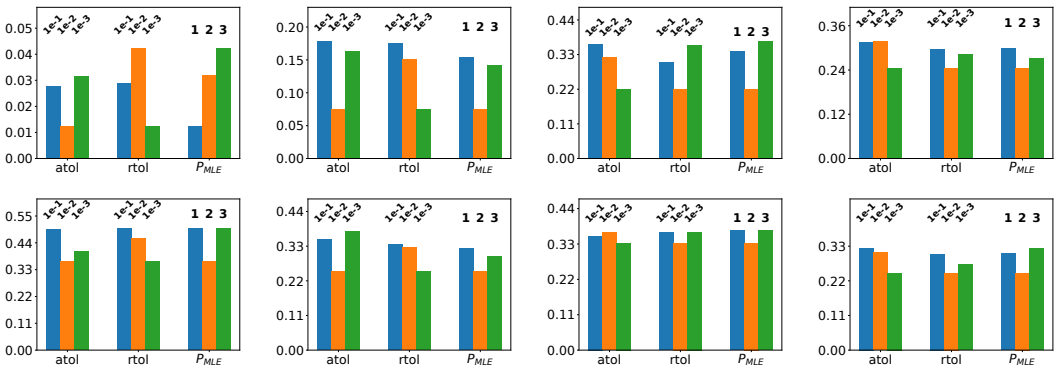

(a) Sines (b) Stocks (c) Energy (d) MuJoCo

Figure 8: The sensitivity of the discriminative score of regluar time-series (the 1st row) and 30% dropped irregular time-series (the 2nd row) w.r.t. some key hyperparameters

5 Conclusions & Future Work

The dominant topic in time-series synthesis is mostly about learning and synthesizing for time-series without missing values, i.e., regular time-series synthesis. However, time-series data in real-world applications is frequently irregular and intermittent, i.e., there are many missing observations and time-series does not have specifically known frequencies. Therefore, we presented how to learn and synthesize for irregular and intermittent time-series data. Our proposed method, IIT-GAN, is based on various advanced deep learning technologies, ranging from GANs to NOCDEs, NCDEs, and so forth. We successfully designed our method after carefully customizing those technologies toward the challenging goal of synthesizing irregular and intermittent time-series. Our experiments, which incorporate various synthetic and real-world datasets, prove the efficacy of the proposed method. In particular, only our method shows reasonable synthesis capabilities when the degree of irregularity and intermittence is high, i.e., a dropping rate of 70% in our experiments.

One important topic in time-series that has not been solved is synthesizing very long time-series, e.g., a time-series length larger than 20,000. Recently, a breakthrough has been proposed for very long time-series classification and forecasting (Morrill et al., 2021). We believe that in the near future, this challenging problem can be solved.

6 ETHICS STATEMENT

Fake data synthesis can be used for several different purposes. One can use our method to protect the privacy of the original data by sharing the synthesized fake data with partners. Others can use our method to augment their insufficient training data. Likewise, we consider that our method has more benefits than risks.

7 REPRODUCIBILITY STATEMENT

We include detailed reproducibility information in Appendix. In particular, we clarify the neural network architectures we used and their best hyperparameter sets for all experiments in our paper. We also submit our source codes and data with appropriate readme descriptions to easily reproduce some selected results due to the 100MB limitation of the supplementary zip file.

REFERENCES

Ahmed Alaa, Alex James Chan, and Mihaela van der Schaar. Generative time-series modeling with fourier flows. In *ICLR*, 2021.

Lei Bai, Lina Yao, Salil S. Kanhere, Xianzhi Wang, and Quan Z. Sheng. Stg2seq: Spatial-temporal graph to sequence model for multi-step passenger demand forecasting. In *Proceedings of the Twenty-Eighth International Joint Conference on Artificial Intelligence, IJCAI-19*, pp. 1981–1987, 7 2019. doi: 10.24963/ijcai.2019/274.

Edward De Brouwer, Jaak Simm, Adam Arany, and Yves Moreau. Gru-ode-bayes: Continuous modeling of sporadically-observed time series. In *NeurIPS*, 2019.

Ricky T. Q. Chen, Yulia Rubanova, Jesse Bettencourt, and David K Duvenaud. Neural ordinary differential equations. In *NeurIPS*. 2018.

Ruizhi Deng, Bo Chang, Marcus A. Brubaker, Greg Mori, and Andreas M. Lehrmann. Modeling continuous stochastic processes with dynamic normalizing flows. In *NeurIPS*, 2020.

Chris Donahue, Julian McAuley, and Miller Puckette. Adversarial audio synthesis, 2019.

Cristóbal Esteban, L. Stephanie Hyland, and Gunnar Rätsch. Real-valued (medical) time series generation with recurrent conditional gans, 2017.

Tak-chung Fu. A review on time series data mining. *Engineering Applications of Artificial Intelligence*, 24(1):164–181, 2011.

Ian Goodfellow, Jean Pouget-Abadie, Mehdi Mirza, Bing Xu, David Warde-Farley, Sherjil Ozair, Aaron Courville, and Yoshua Bengio. Generative adversarial nets. In *NeurIPS*, 2014.

Will Grathwohl, Ricky T. Q. Chen, Jesse Bettencourt, Ilya Sutskever, and David Duvenaud. Ffjord: Free-form continuous dynamics for scalable reversible generative models. 2019.

Alex Graves. Generating sequences with recurrent neural networks, 2014.

Aditya Grover, Manik Dhar, and Stefano Ermon. Flow-gan: Combining maximum likelihood and adversarial learning in generative models. In *AAAI*, 2018.

Ishaan Gulrajani, Faruk Ahmed, Martin Arjovsky, Vincent Dumoulin, and Aaron Courville. Improved training of wasserstein gans. *arXiv preprint arXiv:1704.00028*, 2017.

Shengnan Guo, Youfang Lin, Ning Feng, Chao Song, and Huaiyu Wan. Attention based spatial-temporal graph convolutional networks for traffic flow forecasting. *Proceedings of the AAAI Conference on Artificial Intelligence*, 33(01):922–929, Jul. 2019. doi: 10.1609/aaai.v33i01.3301922.

Rongzhou Huang, Chuyin Huang, Yubao Liu, Genan Dai, and Weiyang Kong. Lsgcn: Long short-term traffic prediction with graph convolutional networks. In *IJCAI*, pp. 2355–2361, 2020.

Junteng Jia and Austin R Benson. Neural jump stochastic differential equations. In *NeurIPS*, 2019.

Patrick Kidger, Patric Bonnier, Imanol Perez Arribas, Cristopher Salvi, and Terry J. Lyons. Deep signature transforms. In *NeurIPS*, 2019.

Patrick Kidger, James Morrill, James Foster, and Terry J. Lyons. Neural controlled differential equations for irregular time series. In *NeurIPS*, 2020.

Patrick Kidger, James Foster, Xuechen Li, Harald Oberhauser, and Terry J. Lyons. Neural sdes as infinite-dimensional gans. *CoRR*, abs/2102.03657, 2021.

Alex Lamb, Anirudh Goyal, Ying Zhang, Saizheng Zhang, Aaron Courville, and Yoshua Bengio. Professor forcing: A new algorithm for training recurrent networks, 2016.

Yaguang Li, Rose Yu, Cyrus Shahabi, and Yan Liu. Diffusion convolutional recurrent neural network: Data-driven traffic forecasting. In *International Conference on Learning Representations (ICLR '18)*, 2018.

Terry J Lyons, Michael Caruana, and Thierry Lévy. *Differential equations driven by rough paths*. Springer, 2007.

Dong Ma, Guohao Lan, Mahbub Hassan, Wen Hu, and Sajal Das. Sensing, computing, and communications for energy harvesting iots: A survey. *IEEE Communications Surveys Tutorials*, 22: 1222–1250, 2020.

Olof Mogren. C-rnn-gan: Continuous recurrent neural networks with adversarial training, 2016.

James Morrill, Cristopher Salvi, Patrick Kidger, and James Foster. Neural rough differential equations for long time series. In *International Conference on Machine Learning*, pp. 7829–7838. PMLR, 2021.

Alec Radford, Luke Metz, and Soumith Chintala. Unsupervised representation learning with deep convolutional generative adversarial networks, 2016.

Gregory C Reinsel. *Elements of multivariate time series analysis*. Springer Science & Business Media, 2003.

Xiaoli Ren, Xiaoyong Li, Kaijun Ren, Junqiang Song, Zichen Xu, Kefeng Deng, and Xiang Wang. Deep learning-based weather prediction: A survey. *Big Data Research*, 23, 2021.

Matthew A Reyna, Chris Josef, Salman Seyedi, Russell Jeter, Supreeth P Shashikumar, M Brandon Westover, Ashish Sharma, Shamim Nemati, and Gari D Clifford. Early prediction of sepsis from clinical data: the physionet/computing in cardiology challenge 2019. In *2019 Computing in Cardiology (CinC)*, pp. Page 1–Page 4, 2019. doi: 10.23919/CinC49843.2019.9005736.

Chao Song, Youfang Lin, Shengnan Guo, and Huaiyu Wan. Spatial-temporal synchronous graph convolutional networks: A new framework for spatial-temporal network data forecasting. *Proceedings of the AAAI Conference on Artificial Intelligence*, 34(01):914–921, Apr. 2020. doi: 10.1609/aaai.v34i01.5438.

Selim Furkan Tekin, Oguzhan Karaahmetoglu, Fatih Ilhan, Ismail Balaban, and Suleyman Serdar Kozat. Spatio-temporal weather forecasting and attention mechanism on convolutional lstms. *arXiv preprint*, 2021.

Aaron van den Oord, Sander Dieleman, Heiga Zen, Karen Simonyan, Oriol Vinyals, Alex Graves, Nal Kalchbrenner, Andrew Senior, and Koray Kavukcuoglu. Wavenet: A generative model for raw audio, 2016.

Laurens Van der Maaten and Geoffrey Hinton. Visualizing data using t-sne. *Journal of machine learning research*, 9(11), 2008.

Zonghan Wu, Shirui Pan, Guodong Long, Jing Jiang, and Chengqi Zhang. Graph wavenet for deep spatial-temporal graph modeling. In *Proceedings of the Twenty-Eighth International Joint Conference on Artificial Intelligence, IJCAI-19*, pp. 1907–1913, 7 2019.

Jinsung Yoon, Daniel Jarrett, and Mihaela van der Schaar. Time-series generative adversarial networks. In *NeurIPS*, 2019.

Bing Yu, Haoteng Yin, and Zhanxing Zhu. Spatio-temporal graph convolutional networks: A deep learning framework for traffic forecasting. In *Proceedings of the Twenty-Seventh International Joint Conference on Artificial Intelligence, IJCAI-18*, pp. 3634–3640, 7 2018. doi: 10.24963/ijcai.2018/505.

A DATASETS

We use 2 simulated (Sines, MuJoCo) and 2 real-world (Stocks, Energy) datasets. Table. 6 shows the statistics of the datasets. All datasets are available online via the link. We note that in some of our datasets, the time-series length N can be varied from one time-series sample to another. However, our framework has no problems in dealing with those varying lengths.

Table 6: Dataset Statistics

Dataset	# of Samples	$\dim(\mathbf{x})$	Average of N	Link
Sines	10,000	5	24 time-points	-
Stocks	3,773	6	24 days	Link
Energy	19,711	28	24 hours	Link
MuJoCo	4,620	14	24 time-points	Link

B ODE/CDE FUNCTIONS IN IIT-GAN

B.1 ENCODER

Our encoder based on NCDEs has the following CDE function f.

Table 7: The architecture of the network f in the encoder

Layer	Design	Input Size	Output Size
1	ReLU(Linear)	$N \times \dim(\mathbf{x})$	$N \times 4\dim(\mathbf{x})$
2	ReLU(Linear)	$N \times 4\dim(\mathbf{x})$	$N \times 4\dim(\mathbf{x})$
3	ReLU(Linear)	$N \times 4\dim(\mathbf{x})$	$N \times 4\dim(\mathbf{x})$
4	Tanh(Linear)	$N \times 4\dim(\mathbf{x})$	$N \times \dim(\mathbf{x})$

B.2 DECODER, DISCRIMINATOR

Our decoder and discriminator based on GRU-ODEs have the following ODE functions. They have the same architecture but their parameters are separated.

Table 8: The architecture of the network g in the decoder

Layer	Design	Input Size	Output Size
1	r_t =Sigmoid(Linear)	$N \times \dim(\mathbf{h})$	$N \times \dim(\mathbf{h})$
	z_t =Sigmoid(Linear)	$N \times \dim(\mathbf{h})$	$N \times \dim(\mathbf{h})$
	u_t =Tanh(Linear)	$N \times \dim(\mathbf{h})$	$N \times \dim(\mathbf{h})$
	$dh = (1 - z_t) * (u_t - h_t)$	$N \times \dim(\mathbf{h})$	$N \times \dim(\mathbf{h})$

Table 9: The architecture of the network q in the discriminator

Layer	Design	Input Size	Output Size
1	r_t =Sigmoid(Linear)	$N \times \dim(\mathbf{x})$	$N \times \dim(\mathbf{x})$
	z_t =Sigmoid(Linear)	$N \times \dim(\mathbf{x})$	$N \times \dim(\mathbf{x})$
	u_t =Tanh(Linear)	$N \times \dim(\mathbf{x})$	$N \times \dim(\mathbf{x})$
	$dh = (1 - z_t) * (u_t - h_t)$	$N \times \dim(\mathbf{x})$	$N \times \dim(\mathbf{x})$

B.3 GENERATOR

Our generator has the following ODE function f in Table 10.

Table 10: The architecture of the network r in the generator

Layer	Design	Input Size	Output Size
1	Softplus(Linear)	$N \times \dim(\mathbf{h}+1)$	$N \times \dim(\mathbf{h})$
2	Softplus(Linear)	$N \times \dim(\mathbf{h}+1)$	$N \times \dim(\mathbf{h})$
3	Softplus(Linear)	$N \times \dim(\mathbf{h}+1)$	$N \times \dim(\mathbf{h})$

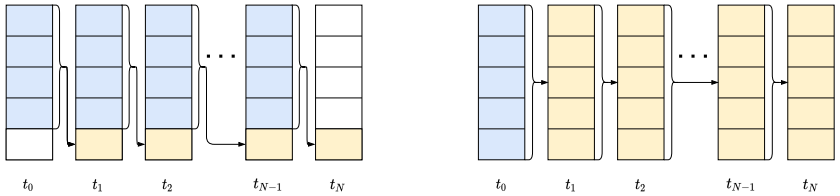

(a) How to calculate the predictive score for the regular time-series synthesis in TimeGAN

(b) How to calculate the predictive score for the irregular and intermittent time-series in this paper

Figure 9: Predictive task according to the data type

C BASELINES

For the regular time-series baseline models, i.e., TimeGAN, RCGAN, C-RNN-GAN, T-forcing, and P-forcing, we use the 3-layer GRU-based neural network architecture with a hidden size that is 4 times larger than the input size. We use or modify the following accessible source codes to run.

- TimeGAN : https://github.com/jsyoon0823/TimeGAN
- RCGAN : https://github.com/3778/Ward2ICU
- C-RNN-GAN : https://github.com/olofmogren/c-rnn-gan
- T-forcing, P-forcing : https://github.com/mojesty/professor_forcing
- GRU-D : https://github.com/zhiyongc/GRU-D

Because ordinary GRUs can not be applied to irregular time-series, we replace the first layer GRU to GRU-D in all those baselines so that the redesigned baseline models, i.e., TimeGAN-D, RCGAN-D, C-RNN-GAN-D, T-forcing-D and P-forcing-D, can process irregular time-series data.

D EVALUATION METRICS

For fair comparison, we reuse the experimental environments of TimeGAN for the discriminative score. However, we found that TimeGAN's predictive task is rather straightforward as shown in Fig. 9 (a). It predicts only one element in yellow from other four past elements in blue. Since only one element is used for evaluation, we found that the original predictive score of TimeGAN can be biased. Instead, our predictive task predicts the entire vector, as shown in Fig. 9 (b), and therefore, our predictive score is measured under much more challenging environments. We use this more challenging predictive score definition for our irregular and intermittent time-series synthesis. We stick to the TimeGAN's definition for the regular time-series experiment for fair comparison but use our challenging predictive score metric for all other experiments.

Table 11: Ablation study of model architecture in Sines

Sines	IIT-GAN (w.o. AE)		IIT-GAN (Flow only)		IIT-GAN (AE only)		IIT-GAN (Full model)	
Metric	Disc.	Pred.	Disc.	Pred.	Disc.	Pred.	Disc.	Pred.
30% dropped	.500	.384	.499	.383	.478	.323	**.363**	**.099**
50% dropped	.500	.523	.499	.445	.477	.409	**.372**	**.101**
70% dropped	.500	.526	.497	.426	.476	.347	**.278**	**.088**

Table 12: Ablation study of model architecture in Stocks

Stocks	IIT-GAN (w.o. AE)		IIT-GAN (Flow only)		IIT-GAN (AE only)		IIT-GAN (Full model)	
Metric	Disc.	Pred.	Disc.	Pred.	Disc.	Pred.	Disc.	Pred.
30% dropped	.498	.207	.492	.140	.493	.133	**.251**	**.021**
50% dropped	.498	.242	.491	.128	.492	.125	**.265**	**.018**
70% dropped	.498	.224	.490	.128	.492	.122	**.230**	**.020**

Table 13: Ablation study of model architecture in Energy

Energy	IIT-GAN (w.o. AE)		IIT-GAN (Flow only)		IIT-GAN (AE only)		IIT-GAN (Full model)	
Metric	Disc.	Pred.	Disc.	Pred.	Disc.	Pred.	Disc.	Pred.
30% dropped	.500	.305	.500	.179	.495	.162	**.333**	**.066**
50% dropped	.500	.365	.499	.160	.499	.135	**.317**	**.064**
70% dropped	.499	.376	.499	.184	.499	.131	**.325**	**.076**

Table 14: Ablation study of model architecture in MuJoCo

MuJoCo	IIT-GAN (w.o. AE)		IIT-GAN (Flow only)		IIT-GAN (AE only)		IIT-GAN (Full model)	
Metric	Disc.	Pred.	Disc.	Pred.	Disc.	Pred.	Disc.	Pred.
30% dropped	.500	.233	.500	.198	.495	.162	**.249**	**.048**
50% dropped	.499	.331	.499	.196	.495	.162	**.270**	**.056**
70% dropped	.499	.326	.499	.200	.496	.146	**.275**	**.051**

E Ablation Studies

We introduce our additional ablation study. We modify our proposed IIT-GAN model by removing its sub-parts to create simpler ablation models. This ablation study shows that the ablation models of IIT-GAN does not perform as well as its full model if any parts are missing.

In the first ablation model, we remove the autoencoder and perform the adversarial training only with our generator and discriminator, denoted IIT-GAN (w.o. AE). In other words, our generation directly outputs raw observations (instead of hidden vectors), which will be fed into our GRU-ODE-based discriminator.

The second ablation model, denoted IIT-GAN (Flow only), has only our CTFP-based generator and we train it with the maximum likelihood training — we note that this construction is the same as training flow-based models. This model is equivalent to the original CTFP model (Deng et al., 2020).

The third ablation model has only the autoencoder, denoted IIT-GAN (AE only). However, we convert it to a variational autoencoder (VAE) model. In the full IIT-GAN model, the encoder produces a set of hidden vectors $\{(t_i, \mathbf{h}_i^{real})\}_{i=0}^N$. In this ablation model, however, this is changed to$\{(t_i, \mathcal{N}(\mathbf{h}_i^{real}, \mathbf{1}))\}_{i=0}^N$, where $\mathcal{N}(\mathbf{h}_i^{real}, \mathbf{1})$ means the unit Gaussian centered at $\mathbf{h}_i^{real}$. The decoder is the same as its full model. We use the variational training for this model.

We summarize their experimental results in Tables 11 to 14. In Table 11, we summarize the results for Sines and the full model greatly outperforms all the ablation models. Among the ablation models, IIT-GAN (AE only) shows the best performance. Similar patterns are observed in other datasets as well.

In Tables 15 to 17, we report the missing ablation study table in the main paper. We reported the ablation study with regular time-series only in the main paper and now report additional results with irregular time-series.

Table 15: Irregular time-series (30% dropped) ablation study

Metric	Method	Sines	Stocks	Energy	MuJoCo
Discriminative	IIT-GAN	**.363**	**.251**	**.333**	.249
Score	w/o Eq. 8	.498	.266	.392	.303
(Lower the Better)	w/o pre-training	.499	.305	.345	**.241**
Predictive	IIT-GAN	**.099**	.021	.066	.048
Score	w/o Eq. 8	.241	**.015**	.064	.061
(Lower the Better)	w/o pre-training	.273	.022	**.061**	**.049**

Table 16: Irregular time-series (50% dropped) ablation study

Metric	Method	Sines	Stocks	Energy	MuJoCo
Discriminative	IIT-GAN	**.372**	.265	**.317**	**.270**
Score	w/o Eq. 8	.500	.323	.381	.274
(Lower the Better)	w/o pre-training	.500	**.209**	.325	**.270**
Predictive	IIT-GAN	**.101**	.018	.064	.056
Score	w/o Eq. 8	.277	.018	**.063**	**.051**
(Lower the Better)	w/o pre-training	.103	**.017**	.071	**.051**

Table 17: Irregular time-series (70% dropped) ablation study

Metric	Method	Sines	Stocks	Energy	MuJoCo
Discriminative	IIT-GAN	**.278**	**.230**	**.325**	.275
Score	w/o Eq. 8	.319	.274	.382	.290
(Lower the Better)	w/o pre-training	.408	.311	.345	**.249**
Predictive	IIT-GAN	.088	**.020**	.076	.052
Score	w/o Eq. 8	**.082**	.025	**.066**	.051
(Lower the Better)	w/o pre-training	.104	.020	.085	**.049**

F SENSITIVITY ANALYSES

We provide performance (discriminative score and predictive score) depending on hyperparameters (i.e. atol (absolute tolerance), rtol (relative tolerance) and P_{MLE} (the period of the MLE training for the generator.)) for each different datasets.

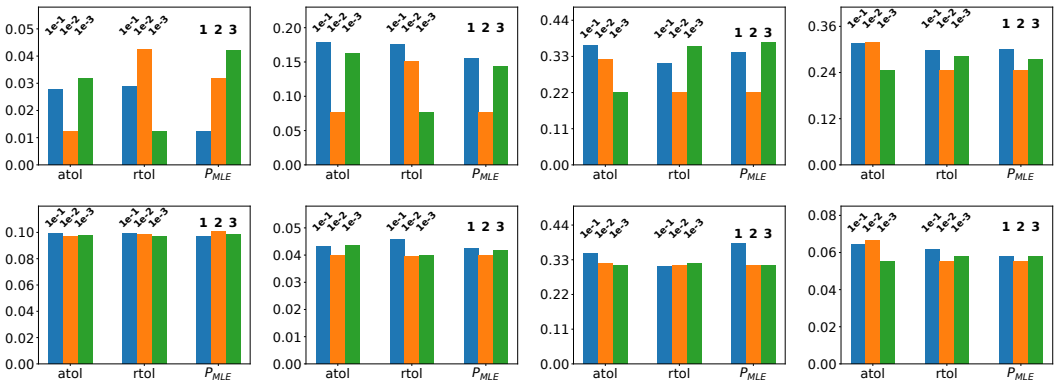

(a) Sines (b) Stocks (c) Energy (d) MuJoCo

Figure 10: The sensitivity of the discriminative score (the 1st row) and predictive score (the 2nd row) w.r.t. some key hyperparameters for regular data

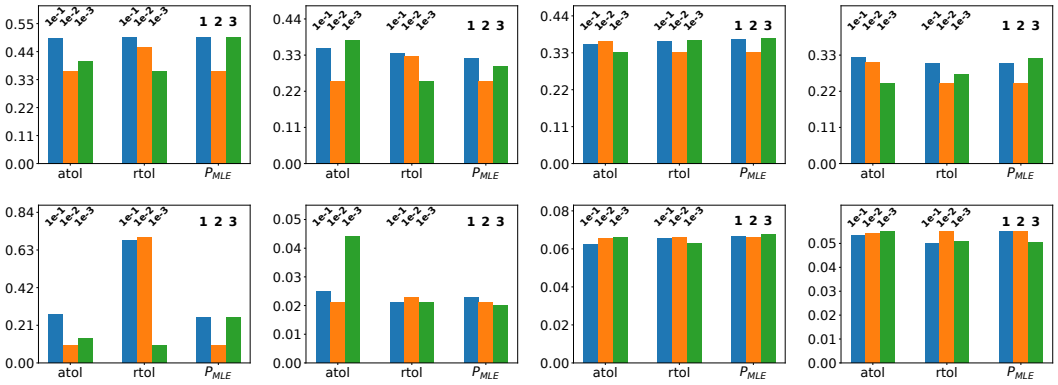

(a) Sines (b) Stocks (c) Energy (d) MuJoCo

Figure 11: The sensitivity of the discriminative score (the 1st row) and predictive score (the 2nd row) w.r.t. some key hyperparameters for irregular data (dropped 30%)

G THE BEST HYPERPARAMTER SET FOR IIT-GAN

- 'atol' means absolute tolerance for the generator.
- 'rtol' means relative tolerance for the generator.
- 'P_{MLE}'means the period of the negative log-density training for the generator.
- 'K_{AE}' means the autoencoder's pre-training iteration numbers.
- 'd-layer' means the number of discriminator's GRU layers.
- 'r-acti' means the last activation function of the decoder.
- 'reg-recon' means the reconstruction regularization for the generator.
- 'reg-kinetic' means the kinetic-energy regularization for the generator.
- 'reg-jacobian' means the Jacobian-norm2 regularization for the generator.
- 'reg-direct' means the directional-penalty regularization for the generator.

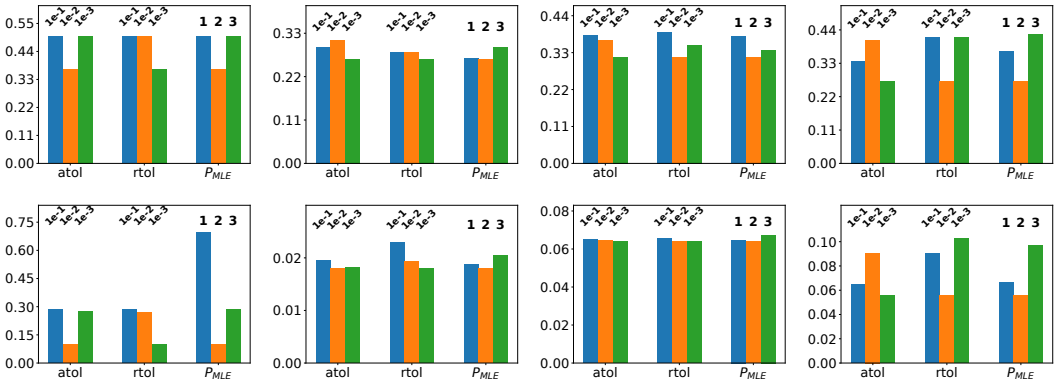

(a) Sines (b) Stocks (c) Energy (d) MuJoCo

Figure 12: The sensitivity of the discriminative score (the 1st row) and predictive score (the 2nd row) w.r.t. some key hyperparameters for irregular data (dropped 50%)

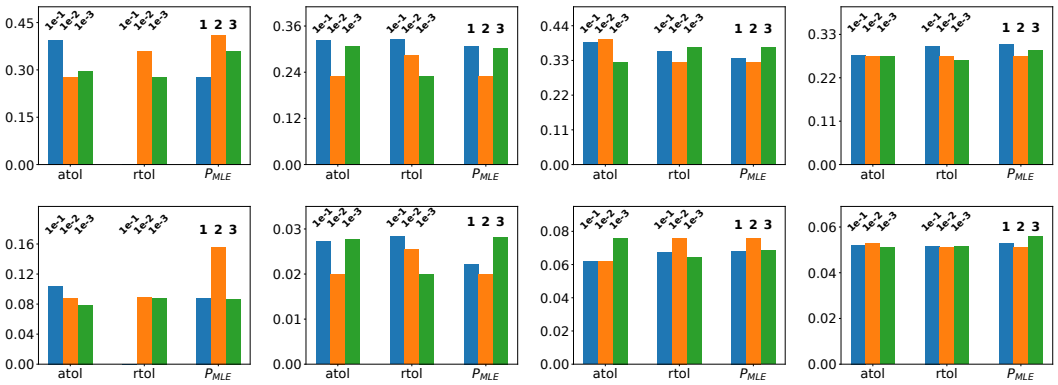

(a) Sines (b) Stocks (c) Energy (d) MuJoCo

Figure 13: The sensitivity of the discriminative score (the 1st row) and predictive score (the 2nd row) w.r.t. some key hyperparameters for irregular data (dropped 70%)

Table 18: The best hyperparameters

method	Data	atol	rtol	P_{MLE}	K_{AE}	d-layer	r-acti	reg-recon	reg-kinetic	reg-jacobian	reg-direct
IIT-GAN (Regular)	Sines	1e-2	1e-3	1	5000	1	softplus	0.01	0.05	0.1	0.1
	Stocks	1e-2	1e-3	2	10000	1	softplue	0.01	0.01	0.05	0.01
	Energy	1e-3	1e-2	2	5000	2	sigmoid	0.01	0.5	0.1	0.01
	MuJoCo	1e-3	1e-2	2	5000	2	sigmoid	0.01	0.05	0.01	0.01
IIT-GAN (Dropped 30%)	Sines	1e-2	1e-3	2	5000	1	softplus	0.01	0.05	0.01	0.01
	Stocks	1e-2	1e-3	2	10000	1	softplue	0.01	None	None	0.05
	Energy	1e-3	1e-2	2	5000	2	sigmoid	0.01	0.5	0.1	0.01
	MuJoCo	1e-3	1e-2	2	2500	2	sigmoid	0.01	0.5	0.1	0.01
IIT-GAN (Dropped 50%)	Sines	1e-2	1e-3	2	5000	2	softplus	0.01	0.05	0.01	0.01
	Stocks	1e-3	1e-3	2	10000	1	softplue	None	0.05	0.01	0.05
	Energy	1e-3	1e-2	2	5000	2	sigmoid	0.01	0.5	0.1	0.01
	MuJoCo	1e-3	1e-2	2	1500	2	sigmoid	0.1	0.1	0.01	0.01
IIT-GAN (Dropped 70%)	Sines	1e-2	1e-3	2	5000	1	softplus	0.01	0.05	0.01	0.01
	Stocks	1e-2	1e-3	1	10000	1	softplue	None	0.05	0.01	0.05
	Energy	1e-3	1e-2	2	2500	2	sigmoid	0.01	0.5	0.1	0.01
	MuJoCo	1e-3	1e-2	2	2500	2	sigmoid	0.01	0.5	0.1	0.01

Table 19: Comparison of model size and training time

	Sines		Stocks		Energy		MuJoCo	
Model	IIT-GAN	TimeGAN	IIT-GAN	TimeGAN	IIT-GAN	TimeGAN	IIT-GAN	TimeGAN
Parameter	41,913	34,026	41,776	48,775	57,104	1,043,179	47,346	264,447
Memory (MB)	1,675	1,419	1,653	1,423	1,839	1,611	1,655	1,546
Training Time (HH:MM)	10:12	2:56	12:20	2:59	10:39	3:37	13:12	3:10

H MODEL SIZE & TRAINING TIME COMPARISON

In Table 19, we report the model size and training time of our method and TimeGAN, one of the best performing baseline. As shown, our model has much smaller numbers of parameters than TimeGAN. However, it take much longer time to train our model than TimeGAN. This is mainly because we need to solve various differential equations, which is not needed for TimeGAN. The memory requirements are more or less the same in both models. Therefore, these exist pros and cons for our method in comparison with the state-of-the-art baseline.

I VISUALIZATIONS WITH T-SNE AND DATA DISTRIBUTION

We introduce additional visualization outcomes in Figs. 14 to 21.

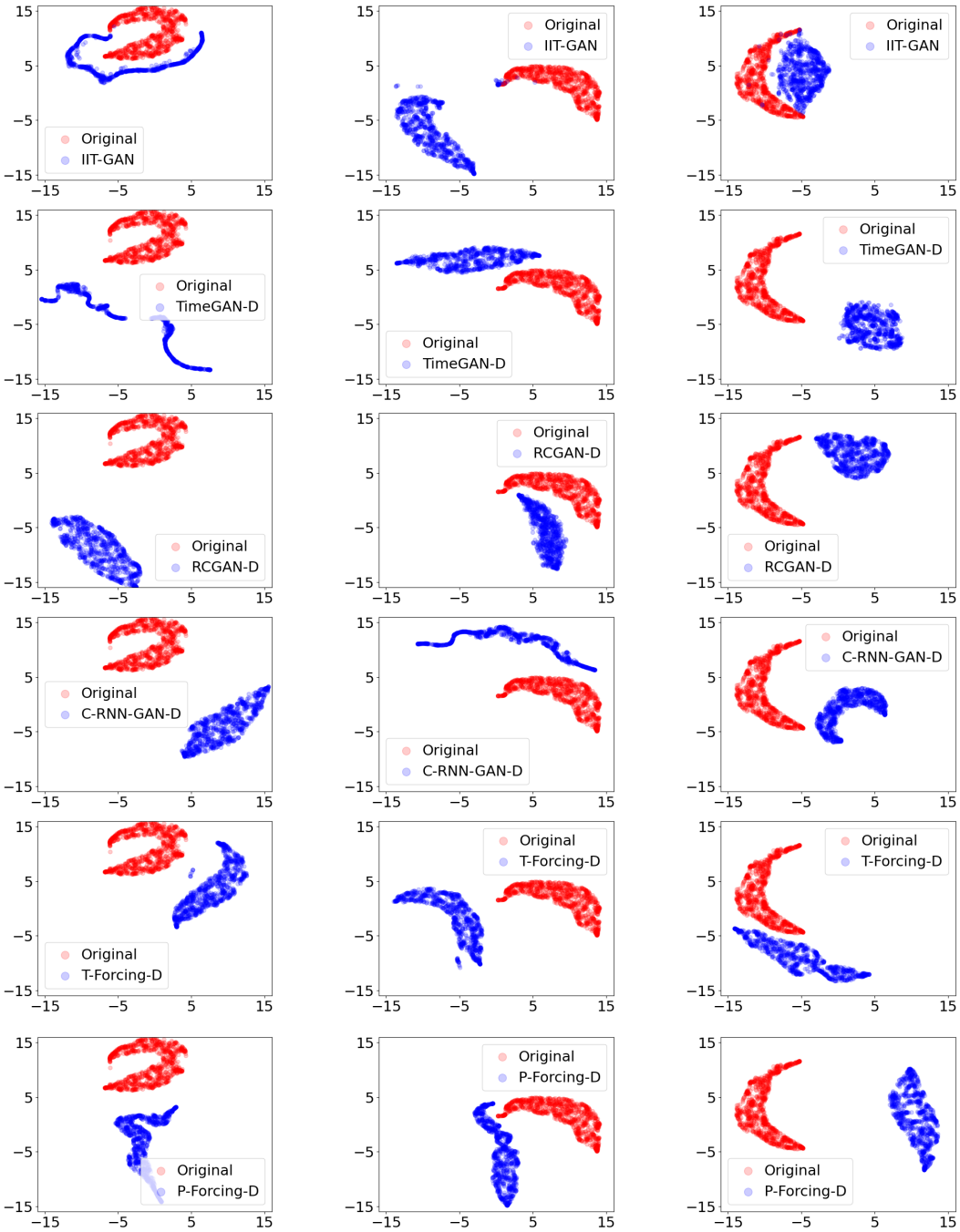

(a) 30% (b) 50% (c) 70%

Figure 14: t-SNE visualization of recovered irregular Sines data (the 1st column is for a dropping rate of 30%, the 2nd column for a rate of 50%, and the 3rd column for a rate of 70%)

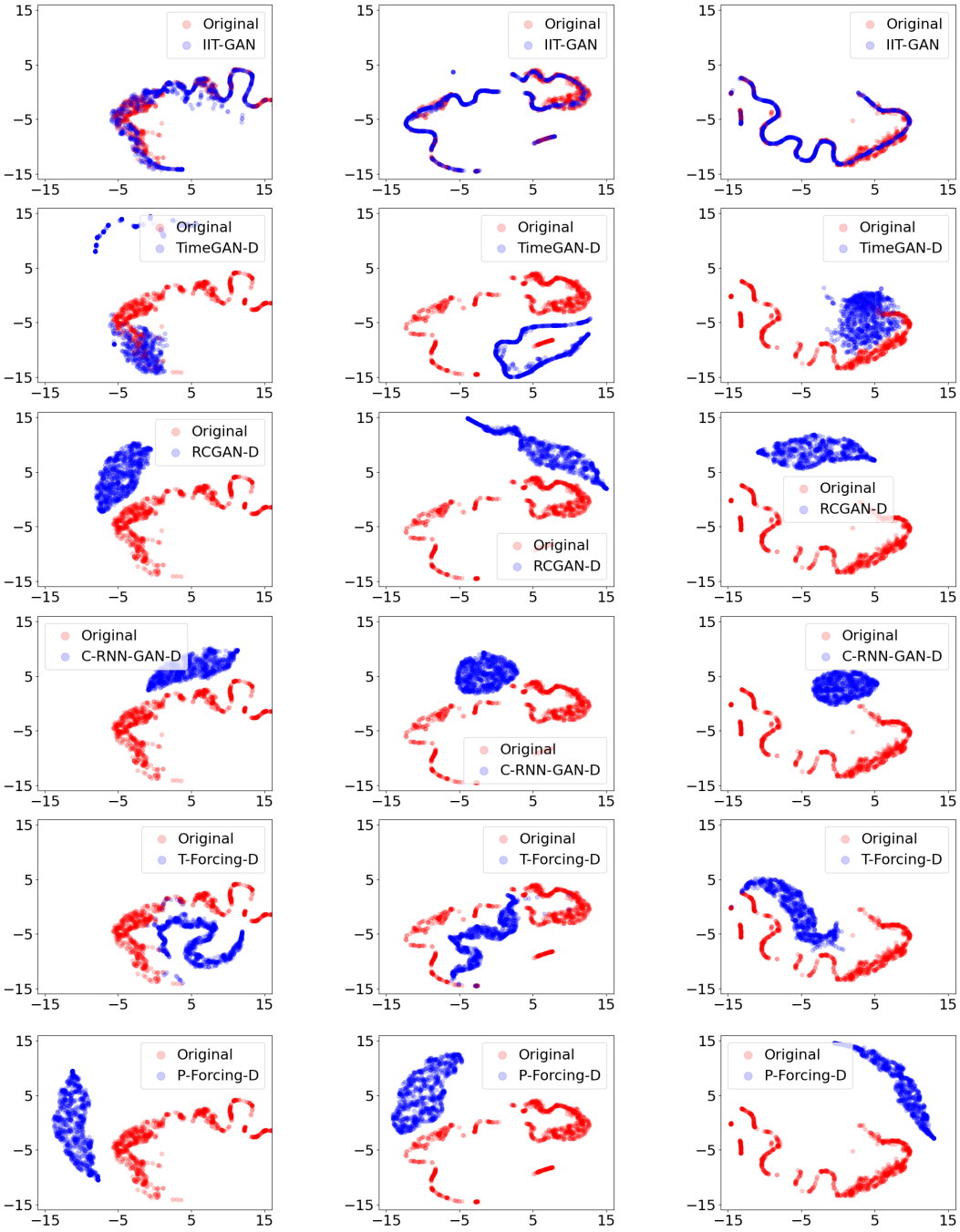

(a) 30% (b) 50% (c) 70%

Figure 15: t-SNE visualization of recovered irregular Stocks data (the 1st column is for a dropping rate of 30%, the 2nd column for a rate of 50%, and the 3rd column for a rate of 70%)

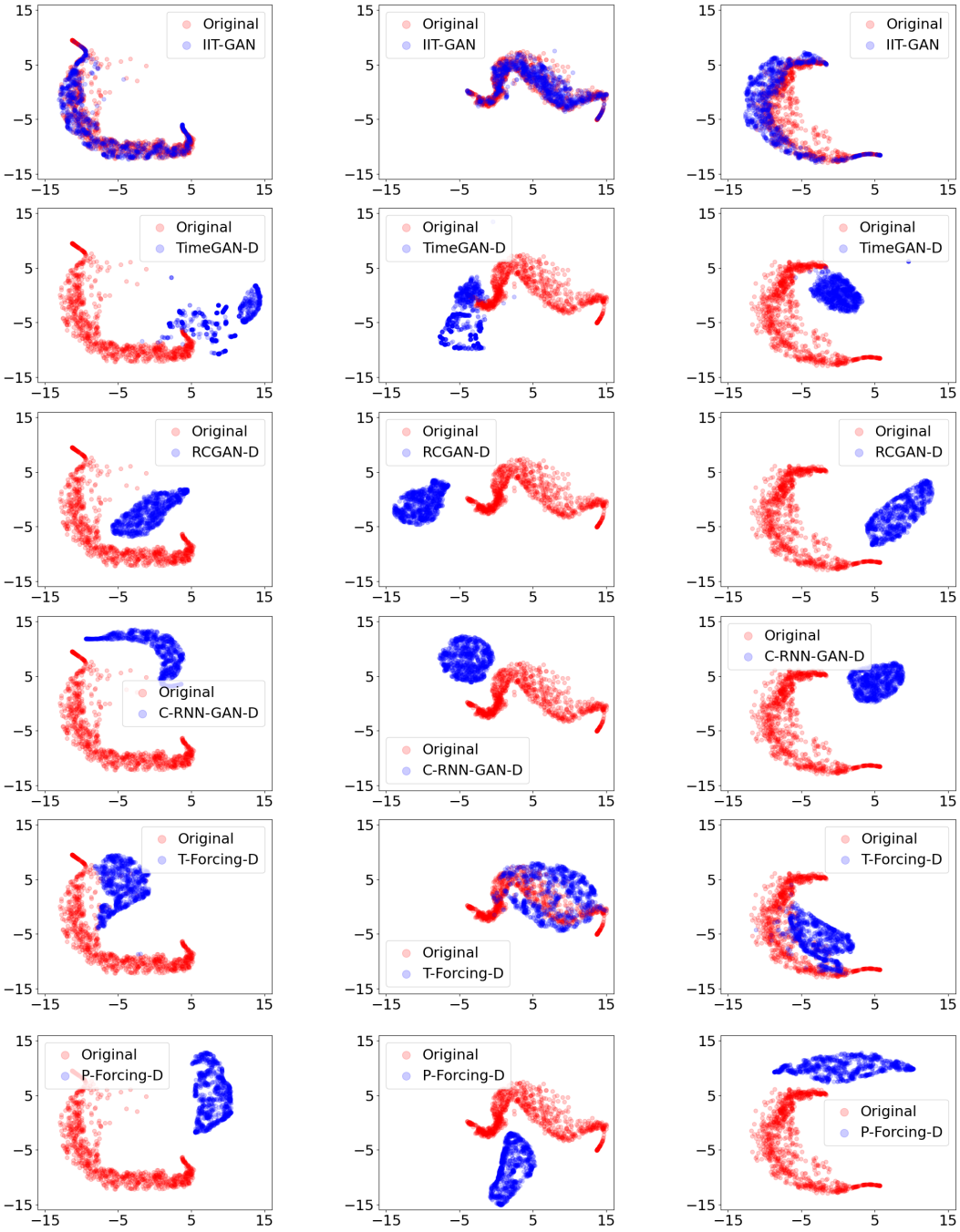

(a) 30% (b) 50% (c) 70%

Figure 16: t-SNE visualization of recovered irregular Energy data (the 1st column is for a dropping rate of 30%, the 2nd column for a rate of 50%, and the 3rd column for a rate of 70%)

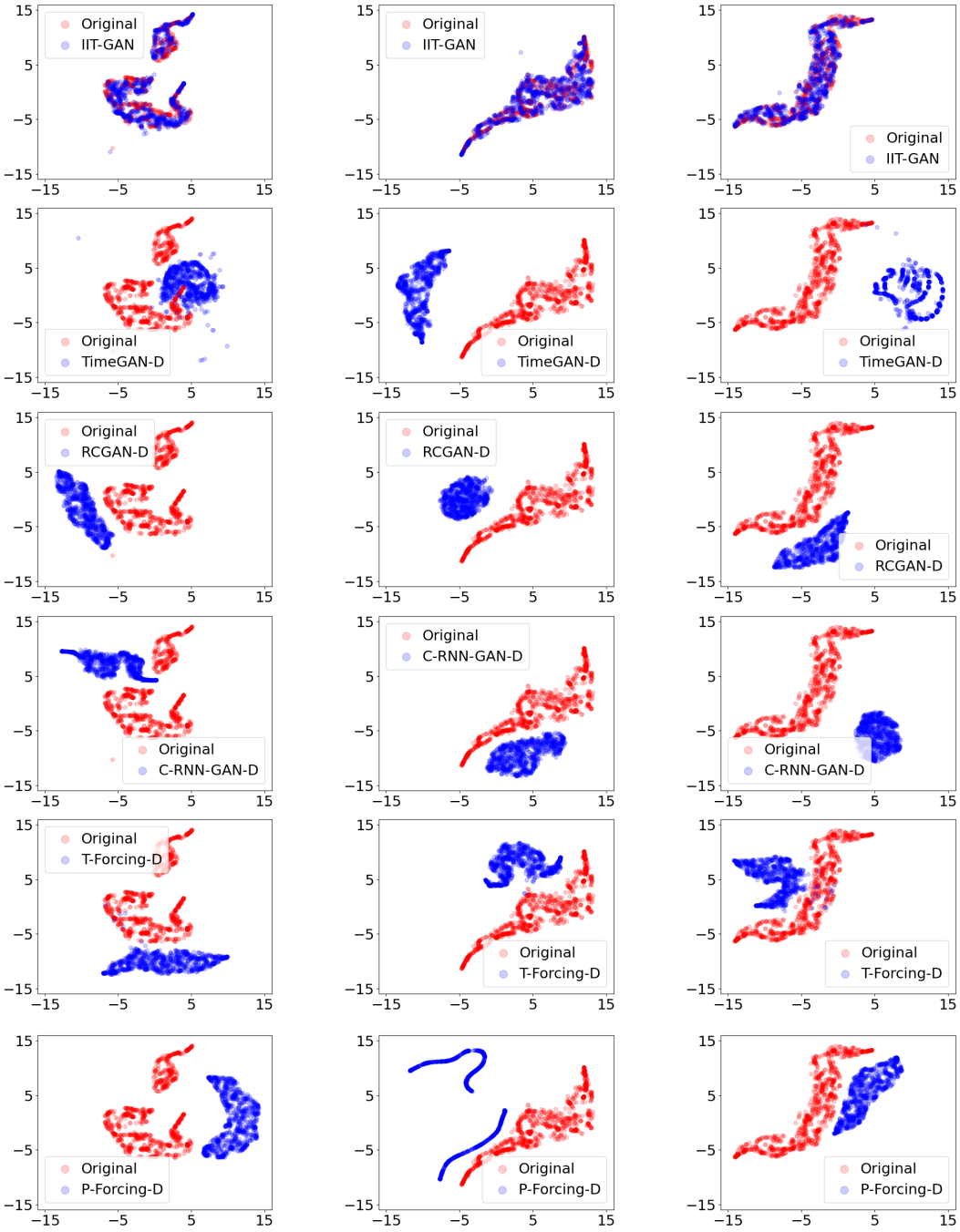

(a) 30% (b) 50% (c) 70%

Figure 17: t-SNE visualization of recovered irregular MuJoCo data (the 1st column is for a dropping rate of 30%, the 2nd column for a rate of 50%, and the 3rd column for a rate of 70%)

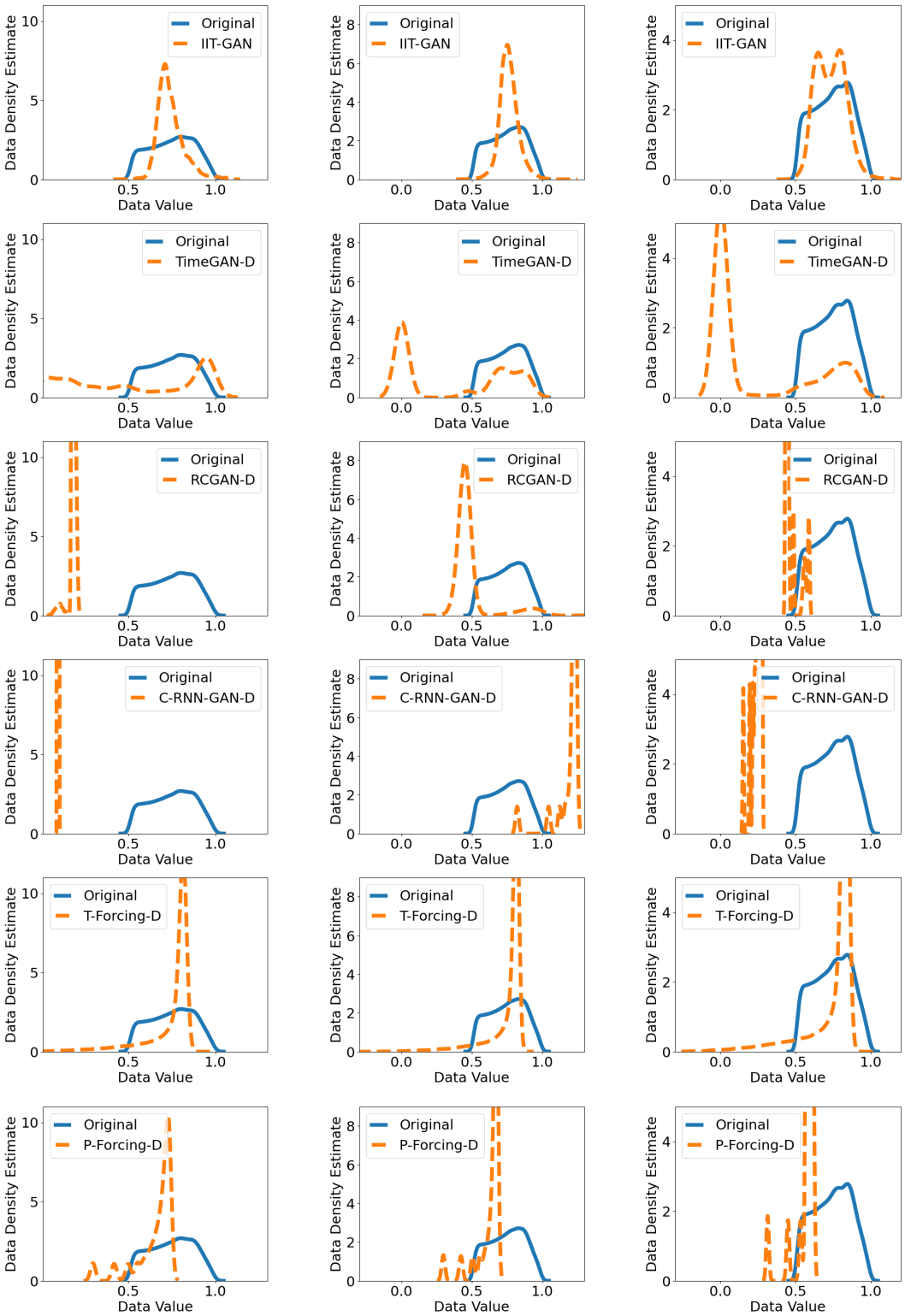

(a) 30% (b) 50% (c) 70%

Figure 18: Distributions of the Sines data (the 1st column is for a dropping rate of 30%, the 2nd column for a rate of 50%, and the 3rd column for a rate of 70%)

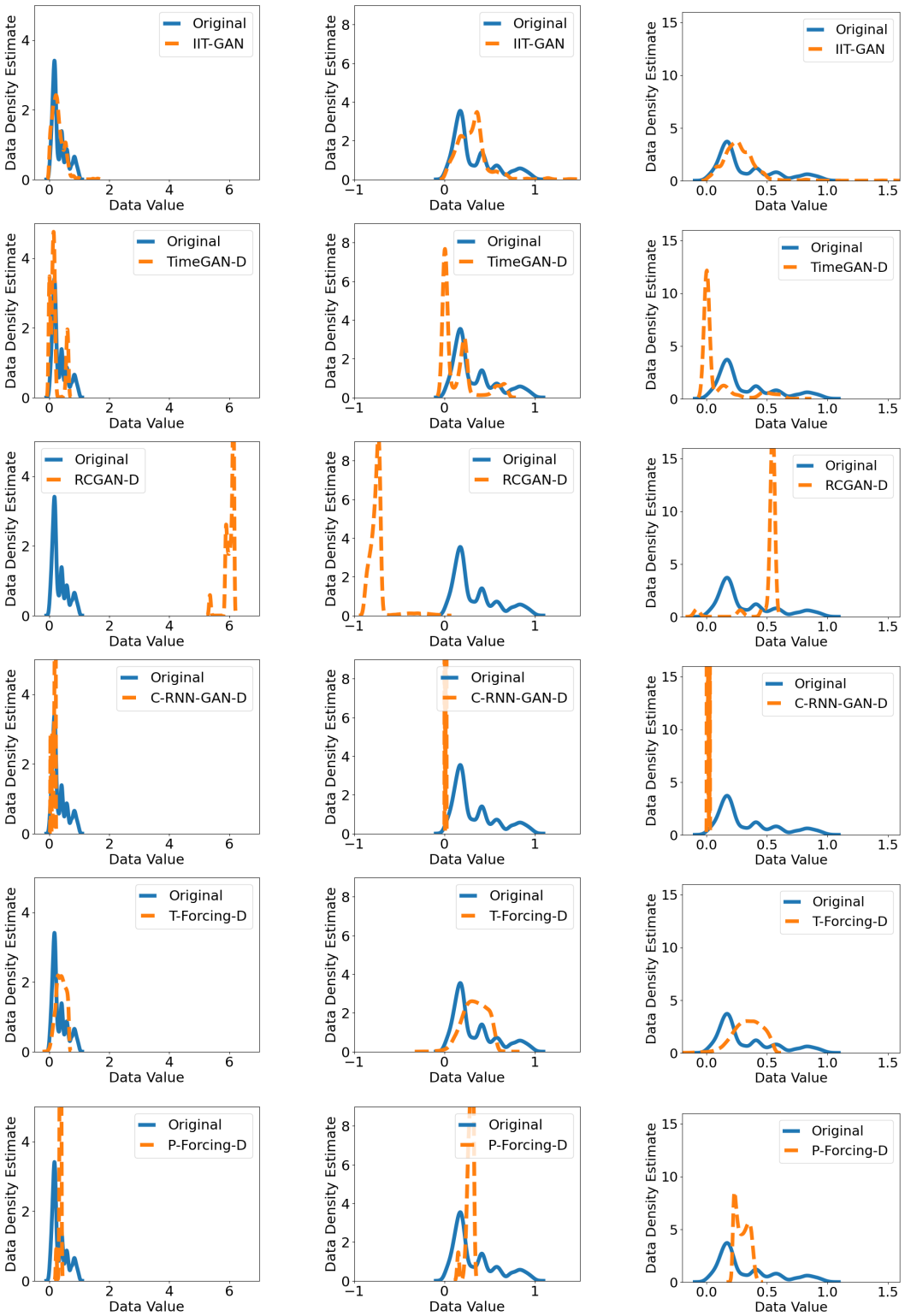

(a) 30% (b) 50% (c) 70%

Figure 19: Distributions of the Stocks data (the 1st column is for a dropping rate of 30%, the 2nd column for a rate of 50%, and the 3rd column for a rate of 70%)

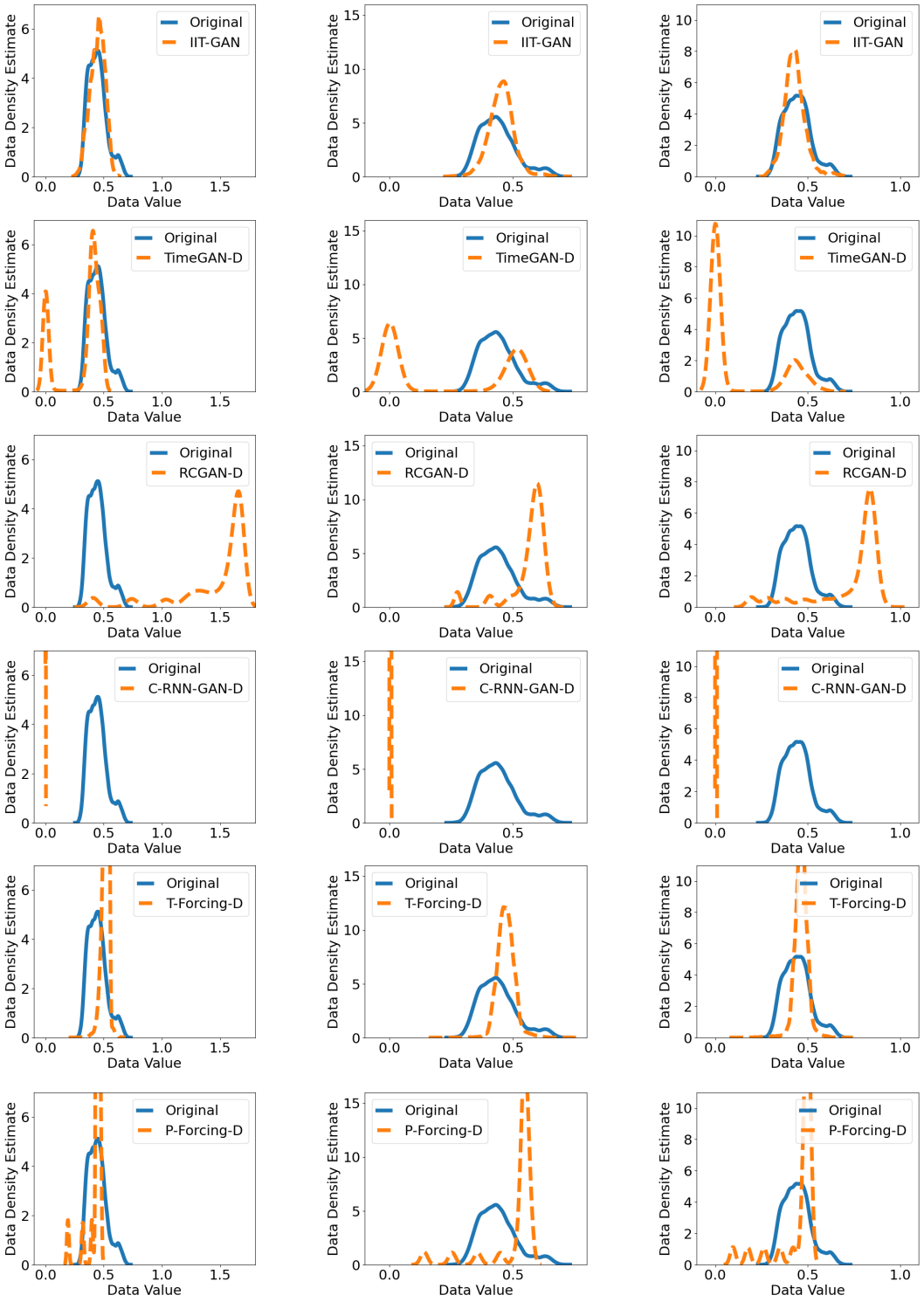

(a) 30% (b) 50% (c) 70%

Figure 20: Distributions of the Energy data (the 1st column is for a dropping rate of 30%, the 2nd column for a rate of 50%, and the 3rd column for a rate of 70%)

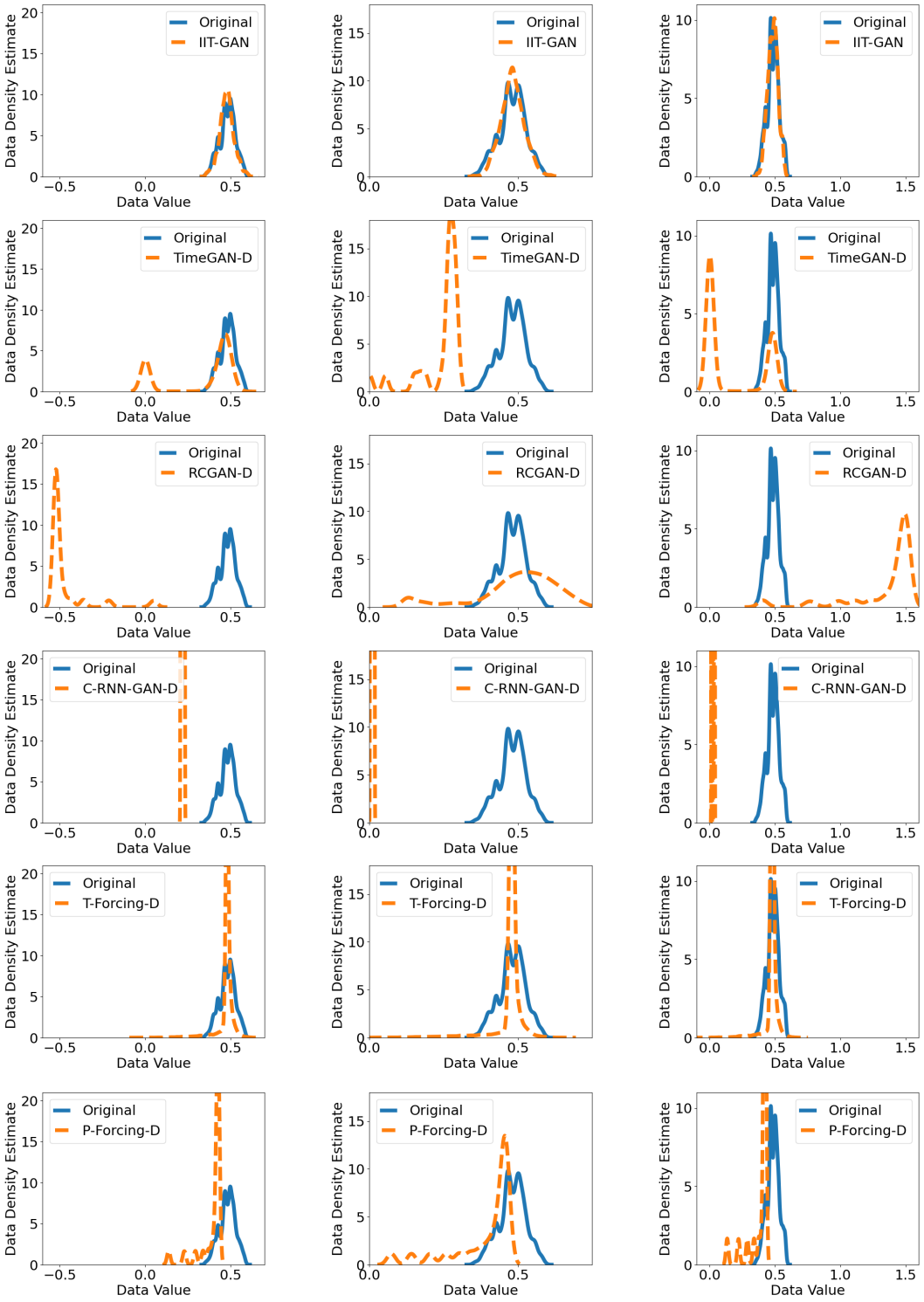

(a) 30% (b) 50% (c) 70%

Figure 21: Distributions of the MuJoCo data (the 1st column is for a dropping rate of 30%, the 2nd column for a rate of 50%, and the 3rd column for a rate of 70%)